Metallogr. Microstruct. Anal. (2013) 2:268–281
DOI 10.1007/s13632-013-0082-8

FEATURE

Quenching and Partitioning Steel Heat Treatment

Li Wang · John G. Speer

Quenching and partitioning (Q&P) steel is a term used to describe a series of C–Si–Mn, C–Si–Mn–Al, or other steels subjected to the recently developed Q&P heat treatment process. The purpose of Q&P steel in the context of automotive structures is to obtain a new type of ultrahigh-strength steel with good ductility to improve fuel economy while promoting passenger safety. With a final microstructure of ferrite (in the case of partial austenitization), martensite, and retained austenite, Q&P steel exhibits an excellent combination of strength and ductility, which permits its use in a new generation of advanced high-strength steels (AHSS) for automobiles. While autobody application represents the first implementation of Q&P on an industrial scale, the heat treatment concept is also applicable to a range of other potential applications.

In 2003, Speer et al. [1] first proposed an approach designated as the Q&P process to exploit novel martensitic steels containing retained austenite (Q&P steel), based on the fact that carbon can diffuse from supersaturated martensite into neighboring untransformed austenite and stabilize it to room temperature. The Q&P steel is first treated by an initial partial or full austenitization and then followed by an interrupted quench to a temperature between the martensite start (M_s) and martensite finish (M_f) temperatures, resulting in untransformed retained austenite, and an anneal or so-called partitioning treatment either at or above the initial quench temperature. With enhanced silicon alloying suppressing cementite precipitation, it is anticipated that retained austenite will be enriched with carbon expected to escape from the supersaturated martensite phase in which it has very low solid solubility. The treatment should then produce a fine acicular aggregate of carbon-depleted and potentially carbide-free martensite laths interwoven with retained austenite stabilized by carbon enrichment. As a result, with a composition of 0.2% C, 1–1.5% Al, and 1–1.5% Mn, Q&P steel [2] shows an ultrahigh strength of 1000–1400 MPa (145–200 ksi) with adequate ductility of 10–20%; property advancements continue to be made through research on this emerging technology. Early investigations [1] also proposed a corresponding thermodynamic model for Q&P steel and its heat treatment, which is now referred to as constrained carbon equilibrium [3].

Since first proposed in 2003, Q&P steel has gained interest for its potential to enhance properties of strength and ductility with compositions similar to transformation-induced plasticity (TRIP) steel and has been proposed as a third-generation automotive steel (Fig. 1) [4]. Many researchers [5–17] have investigated the relationship between properties and microstructures of Q&P steels subjected to various heat treatments and showed that the ultrahigh strength of Q&P steel results from martensite laths, while its good ductility is attributed to TRIP-assisted behavior of retained austenite during deformation. De Moor et al. [14] examined the stability of retained austenite and showed that the TRIP effect occurs in Q&P steels, thereby effectively contributing to the significant strain hardening. Santofimia et al. [15, 16] and Takahama et al. [17] analyzed microstructural evolution during annealing

Editor's Note The following is a preview chapter from the upcoming volume *Steel Heat Treating Fundamentals and Processes,* Volume 4A, *ASM Handbook,* Jon Dossett and George Totten, editors. The volume is scheduled for publication later this year.

L. Wang
Automotive Steel Research Institute and Baoshan Iron & Steel Company, Ltd, Shanghai, China

J. G. Speer
Colorado School of Mines, Golden, CO, USA

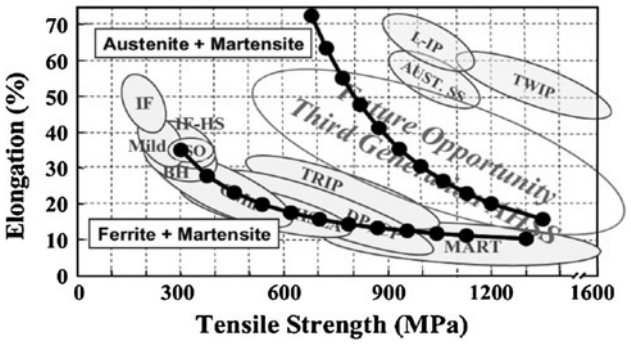

Fig. 1 Predicted potential for austenite/martensite mixtures to achieve property targets beyond those of ferrite/martensite mixtures for third-generation advanced high-strength sheet steels. *Source* [4]

Table 1 Chemical compositions of current-generation Q&P steels

Chemical composition, wt%					
C	Mn	Si	Al	P	S
0.15–0.30	1.5–3.0	1.0–2.0	0.02–0.06	<0.015	<0.01

by using a model considering the influence of martensite–austenite interface migration on the kinetics of carbon partitioning and indicated that different interface mobilities lead to profound differences in the evolution of microstructures during the partitioning process. In addition, processing opportunities for Q&P steels were discussed by Matlock and Speer [18] and Thomas et al. [19, 20] based on the considerations in the application of the Q&P concept to automotive AHSS production. Additional work has been subsequently published by multiple research groups. In 2009, the world's first industrially processed Q&P cold rolled sheet steel was produced by Baosteel, having a tensile strength over 980 MPa (142 ksi) and ductility over 15%. In 2012, Q&P steel with a tensile strength of 980 MPa was successfully commercialized [21–23], and a 1180 MPa (170 ksi) tensile strength Q&P sheet grade is under development. This article provides an overview of important background and product characteristics, with a focus on the automotive sheet steel application that has now reached commercialization. The Q&P heat treating concept has broader potential and may be extended to other products and applications in the future.

Chemical Composition and Annealing Process

The chemical compositions of typical Q&P steels are listed in Table 1. The Q&P steels are hypoeutectoid iron–carbon alloys that typically contain 0.15–0.30% C by weight, similar to TRIP steels. The Q&P steels also contain alloying elements such as silicon that prevent the

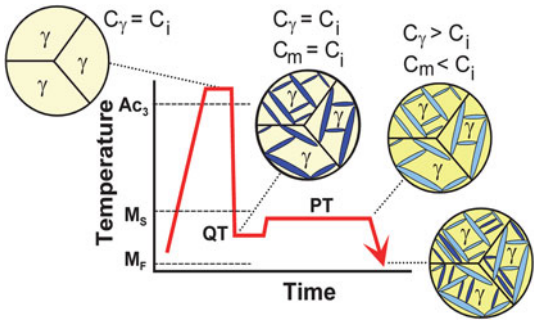

Fig. 2 Schematic illustration of the thermal profile and phase-transformation behavior of Q&P steels. *QT* quenching temperature, *PT* partitioning temperature

precipitation of the cementite phase (Fe_3C), which is present in typical steels at room temperature. This maintains the high carbon concentration in the austenite phase, which becomes stable at room temperature. Carbon content in current Q&P steels is limited to 0.15–0.30 wt% due to weldability concerns. As shown in Table 1, the manganese content in Q&P steels is relatively high, to enhance hardenability and austenite stability. Silicon is used to stabilize the austenite phase during continuous annealing and at room temperature, because silicon significantly increases the carbon activity in both ferrite and austenite and decreases carbon solubility in ferrite. As a result, silicon inhibits the formation of cementite during the partitioning stage. Because Q&P steels have already exhibited an excellent balance between ultrahigh strength and high ductility, other alloying elements have not been necessary, although opportunity is likely available to use microalloying and other concepts for additional enhancements.

Thermal Profile and Phase Transformation

The continuous annealing process and consequent phase-transformation behaviors of Q&P steels are schematically shown in Fig. 2. To produce Q&P steel with ultrahigh strength and excellent ductility, a unique annealing process is conducted to obtain the appropriate phase distribution. First, the steel is heated to a temperature above Ac_3 (annealing temperature), where the material is composed of austenite. The material is then slowly cooled to a temperature below Ar_3 (slow cooling temperature, or SC), which is approximately 740 °C (1360 °F) for the 980 MPa (142 ksi) steel grade, to allow the formation of a certain amount of proeutectoid ferrite. The ferrite phase plays a significant role in the improvement of ductility of the 980 MPa material. The fraction of ferrite and martensite phases can be adjusted by precisely controlling SC. After slow cooling, the steel is then quenched to a temperature between M_s and M_f (quenching temperature) with a cooling rate higher than 50 °C/s (90 °F/s), wherein austenite

transforms (partially) to martensite. The fractions of austenite and martensite can be controlled by this interrupted quenching process. After quenching, the steel is usually reheated to a higher temperature (partitioning temperature) and held for a couple of minutes. In a typical steel alloy, the supersaturated carbon in martensite would lead to cementite precipitation. However, the high content of silicon prevents the formation of cementite. Consequently, the excess carbon in the martensite phase partitions into the remaining austenite, because austenite with a face-centered cubic structure exhibits much higher carbon solubility than martensite with a body-centered cubic structure. Finally, the stable carbon-enriched austenite is retained when the steel is cooled to room temperature. After this unique heat treatment, the final microstructure composed of ferrite, martensite, and retained austenite is achieved. The key annealing considerations to produce Q&P steels are that fast cooling is needed, and, at the same time, the quench arrest temperature must be easily controlled below the M_s temperature.

Microstructure and Mechanical Properties

The microstructure of commercial Q&P steels is composed primarily of martensite (50–80%) formed during quenching, and ferrite (20–40%) formed from the austenite phase during slow cooling, as well as dispersed retained austenite (5–10%) stabilized by carbon enrichment during partitioning. Reduced fractions of ferrite can be used in higher-strength products. Example micrographs taken with a scanning electron microscope and a light optical microscope can be seen in Fig. 3. Small nodules of retained austenite are found, and films of austenite are also present in the lath martensite. The fine Q&P microstructure is usually not well resolved by light optical microscopy. Some additional aspects related to microstructure are also included in the following sections.

Mechanical Properties

Carbon-enriched metastable retained austenite is considered beneficial because TRIP during deformation, that is, the TRIP phenomenon, can contribute to work hardening, formability, and fracture toughness. During deformation, the dispersed retained austenite progressively transforms to harder martensite, which creates a high work-hardening rate, even at higher strain levels. A typical strain–stress curve is shown in Fig. 4. It can be seen that with a tensile strength of 980 MPa (142 ksi), the total elongation of Q&P steel is approximately 20%. Mechanical properties of industrially produced Q&P steels are listed in Table 2 for minimum tensile strength levels of 980 and 1180 MPa (142 and 170 ksi).

Applications

The Q&P steels with ultrahigh strength and excellent ductility, or formability, are well suited to help reduce weight of car bodies, with the added advantage of enhanced occupant safety. The work-hardening rates of Q&P steels are substantially higher than for conventional high-strength steels (HSS), providing significant stretch-forming capability. Compared to most other HSS with the same tensile strength, Q&P steels exhibit much higher formability; hence, they are particularly well suited for automotive structural and safety parts such as cross members, longitudinal beams, B-pillar reinforcements, sills, and bumper reinforcements, which cannot be cold formed using conventional HSS with similar strength levels. Some typical automotive parts produced from Q&P steels are shown in Fig. 5. This family of steels is at an early stage of industrial implementation and may find its way into other

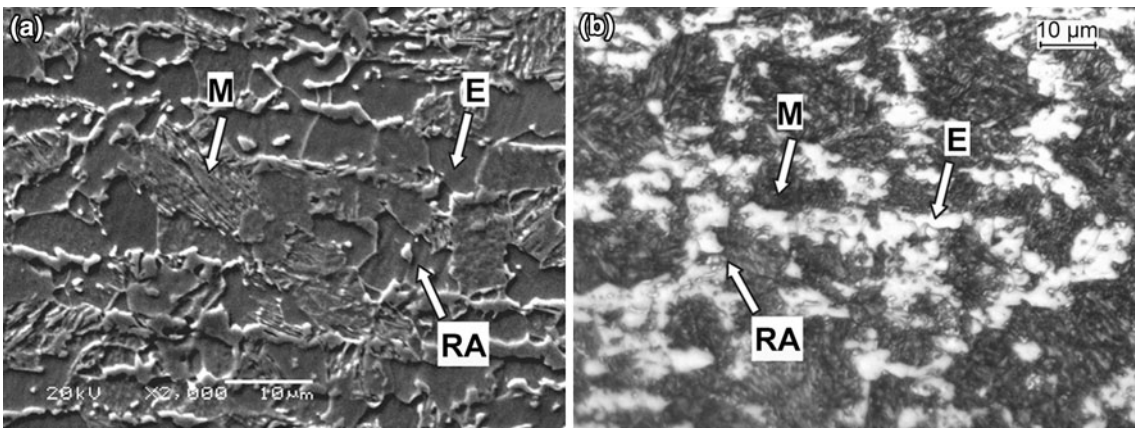

Fig. 3 Microstructure of Q&P steel obtained using (**a**) scanning electron microscopy and (**b**) light optical microscopy. *M* martensite, *F* ferrite, *RA* retained austenite

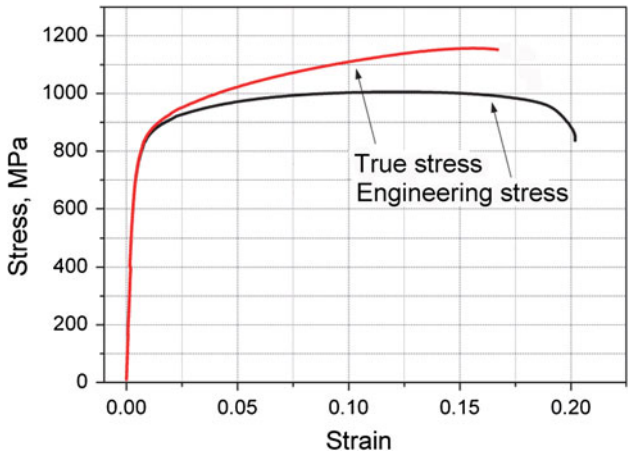

Fig. 4 Strain–stress curve of industrially produced 980 MPa (142 ksi)-grade Q&P steel

Table 2 Typical mechanical property ranges for current-generation Q&P steels

Steel	Yield strength		Tensile strength		Elongation, %
	MPa	ksi	MPa	ksi	
Q&P 980	650–800	95–115	980–1050	140–150	17–22
Q&P 1180	950–1150	140–170	1180–1300	170–190	8–14

high-strength components for both automotive and other applications.

Forming

The Q&P steels offer high ductility for their tensile strength. For example, cold rolled Q&P 980 has a total elongation of approximately 20%, and cold rolled Q&P 1180 has a total elongation of approximately 12%. Figure 6 shows typical forming-limit curves for cold rolled Q&P 980, dual-phase (DP) 780, and DP 980 steels. The formability of Q&P 980 is superior to that of DP 980 steel and reaches to the level of DP 780.

Dynamic Tensile Properties

Besides quasi-static tensile testing results, dynamic tensile testing of sheet steels is also important for more precise evaluation of vehicle crashworthiness in the automotive industry. Positive strain-rate sensitivity, that is, strength increases with strain rate, offers a potential for improved energy absorption during a crash event. The results of dynamic tensile testing of Q&P 980 are shown in Fig. 7. The results confirm that Q&P steel exhibits positive strain-rate sensitivity.

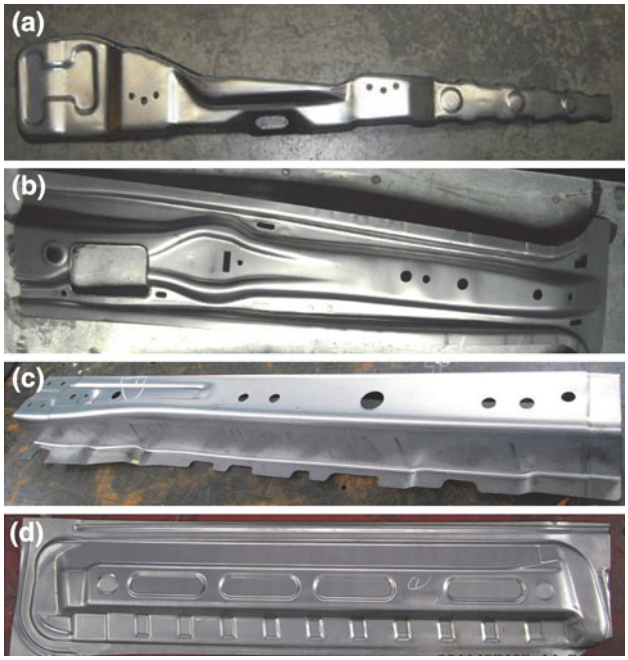

Fig. 5 (**a**) B-pillar reinforcement left/right. Material: 980 Q&P steel; gage: 2.0 mm (0.08 in.). (**b**) B-pillar inner. Material: 980 Q&P; gage: 1.2 mm (0.05 in.). (**c**) Side member front floor left. Material: 980 Q&P; gage: 1.8 mm (0.07 in.). (**d**) Door panel inner left/right. Material: 980 Q&P; gage: 1.0 mm (0.04 in.)

Application Properties of Q&P Steels

Hole-Expansion Ratio (HER) of Q&P Steels

One of the concerns for AHSS in stamping operations is the failure of sheared edges in stretching modes. The HER is usually used to characterize the sheared-edge stretchability. The HER of Q&P 1180 and Q&P 980 compared to DP 980 is shown in Fig. 8. For either punched or machined edges, Q&P 1180 shows higher HER than Q&P 980 and DP 980, while Q&P 980 shows similar HER as DP 980. One possible explanation of the high HER of Q&P 1180 is its high yield strength/tensile strength ratio and uniform microstructure. It should be noted that the HER can be significantly lower for punched holes compared with machined holes. This probably is due to the reduced local elongation of the multiphase steels, which can have interfacial failure between the ductile ferrite matrix and the harder phases.

Shear Fracture Behavior of Q&P Steels

Shear fracture can happen during stretching over the die radii for some part geometries at strains below the conventional forming limit of the material; thus, computer simulations often fail to predict this type of fracture using the conventional forming limit as the failure criterion.

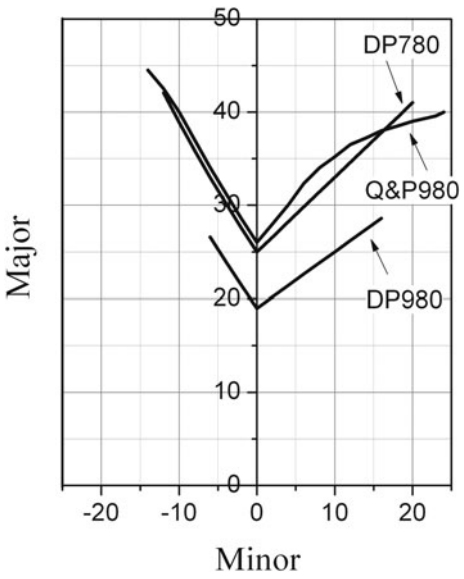

Fig. 6 Forming-limit curves for Q&P 980, DP 780, and DP 980. Thickness: 1.2 mm (0.05 in.)

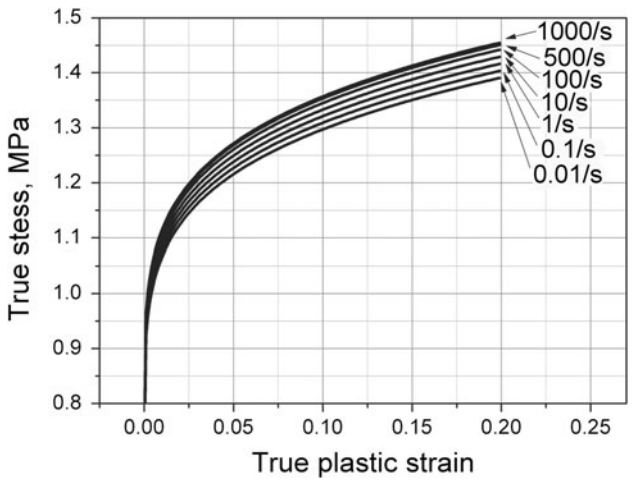

Fig. 7 Dynamic tensile testing results for Q&P 980

Shear fracture is another manufacturing issue to address for AHSS. The shear fracture performance of Q&P steel was evaluated by the bending-under-tension test, and a critical *R*/*t* value was determined according to the criterion developed by Hudgins [24]. The critical *R*/*t* data for Q&P 980, DP 980, TRIP 780, and data for the commercial steels tested by Hudgins [24] are presented together in Fig. 9 as a function of the tensile strength. The results illustrate that the commercial steels generally show increasing critical *R*/*t* values with increasing strength in the range of tensile strength from 400 to 1100 MPa (60 to 160 ksi). Interestingly, the Q&P 980 exhibited lower critical *R*/*t* values than those steels having 780 and 980 MPa (110 and 142 ksi) strength levels and critical *R*/*t* values close to those of other steels having 600 MPa (87 ksi) strength levels. Thus, the

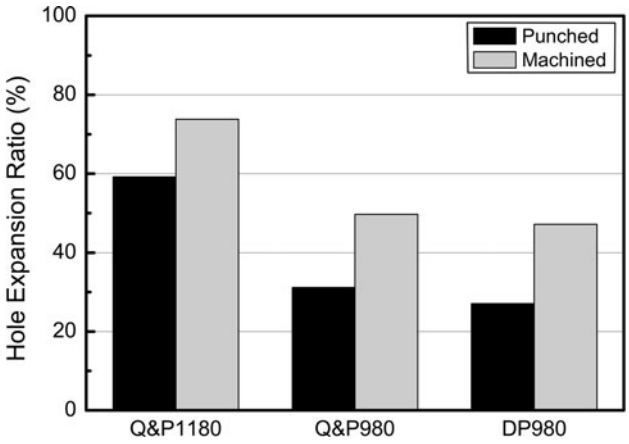

Fig. 8 HER of Q&P steels compared to DP 980 for punched or machined holes

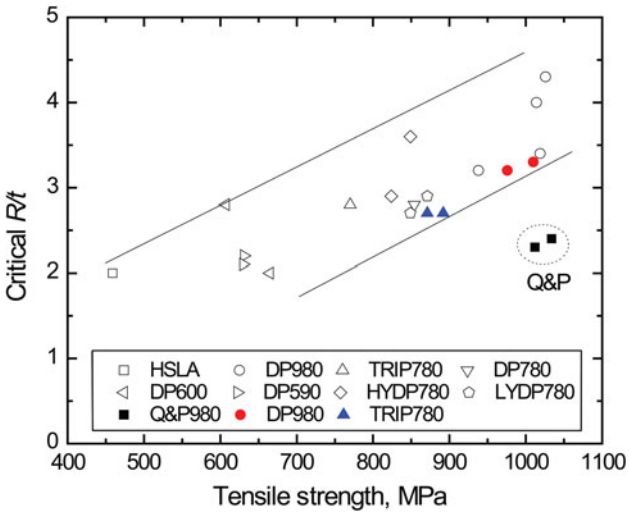

Fig. 9 Comparison of the critical *R*/*t* values for Q&P 980 and other HSS. Unfilled points are from the work of Hudgins. *Source* [21]

shear fracture performance of Q&P 980 should be better than that of some DP 980, DP 780, and TRIP 780 steels.

Springback Behavior of Q&P Steels

Many reports indicate that springback problems are much greater for AHSS than for traditional HSS. The springback angle of 1.2 mm (0.05 in.) Q&P 980 was thus compared to 1.2 mm DP 980 using the bending-under-tension test. A strong linear relationship between springback angle and normalized back force (back force/tensile strength) was found, as shown in Fig. 10. With increasing back force, the springback angle decreases. Almost no difference was observed between Q&P 980 and DP 980 when a 5 mm (0.2 in.) radius die was used. The Q&P 980 exhibited smaller springback angles than DP 980 when a 12.7 mm (0.5 in.) radius die was used, suggesting that Q&P 980 may

have better springback performance than DP 980 in some situations.

Mechanical Behavior and Stability of Retained Austenite

An essential principle in the Q&P process is to maintain suitable stability of retained austenite through optimizing chemical composition (alloy elements such as carbon, manganese, silicon, etc.) [25], grain refinement [26], and phase morphology [25].

Mechanical Properties

Engineering stress–strain curves obtained on longitudinal specimens at six different temperatures are illustrated in Fig. 11. The specimens showed continuous yielding behavior, which can be interpreted as the result of the high density of dislocations introduced by martensite. The M_s^σ temperature for strain-induced transformation can characterize retained austenite stability. When the tensile temperature is in the range of M_s to M_s^σ, plastic deformation of the austenite involves stress-induced transformation at pre-existing nucleation sites, with a load drop evident during yielding. When the temperature is between M_s^σ and M_d, the stability of the retained austenite is expected to increase, perhaps leading to a transition from stress-induced transformation to strain-induced transformation. The symbol M_d refers to the minimum temperature where no martensite transformation occurs during deformation. The deformation-induced martensitic transformation (DIMT) of austenite is desired at higher strains to enhance the tensile ductility. The M_s^σ temperature of most low-alloy TRIP steels is typically in the range of −10 to +10 °C (14–50 °F) [17]. However, according to interpretation of the yielding behaviors in Fig. 11, the M_s^σ temperature of the examined Q&P steel is confirmed to be below −40 °C (−40 °F). The retained austenite in the Q&P steel is thus believed to be relatively more stable compared to that in TRIP steel, which is considered beneficial to formability.

Figure 12 demonstrates the effect of testing temperature on yield strength (YS), ultimate tensile strength (UTS), and total elongation (TEL) of a Q&P 980 steel. It is observed that the YS remains relatively stable over the test temperature range in comparison to the UTS; the decrease in UTS is up to approximately 104 MPa (15 ksi) with an increase in test temperature from −40 to 60 °C (−40 to 140 °F), while the YS is rather stable. This strengthening effect at low temperature can be attributed to two factors: the result of reduction of thermally activated flow and the transformation of retained austenite, which is further elucidated subsequently. The TEL also varies significantly with testing temperature. The maximum value of TEL appears to be in the range of 0–20 °C (32–68 °F) for this steel, while TEL decreases slightly with increasing temperature above 20 °C. The austenite chemical composition and grain-size distribution influence its stability, and retained austenite with finer particle size and greater carbon concentrations is more stable and resists transformation during deformation. Further increasing the stability of retained austenite by increasing the testing temperature by 20 °C (36 °F) apparently begins to deteriorate the ductility of this steel.

Retained Austenite Transformation

Retained austenite stability is characterized at different uniaxial tensile testing temperatures by observing deformation and transformation behavior of austenite using

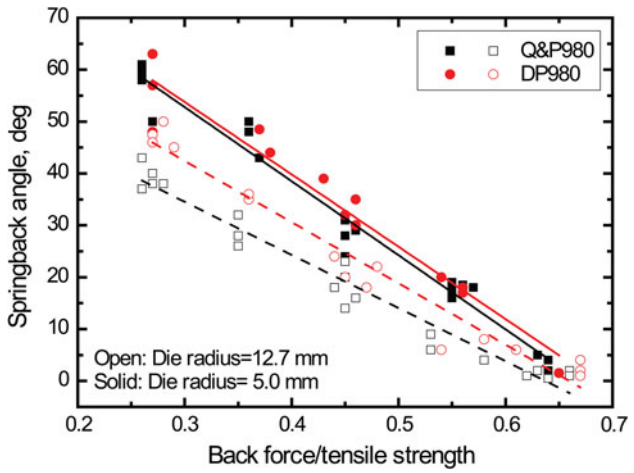

Fig. 10 Comparison of springback angle between Q&P 980 and DP 980 using the bending-under-tension test

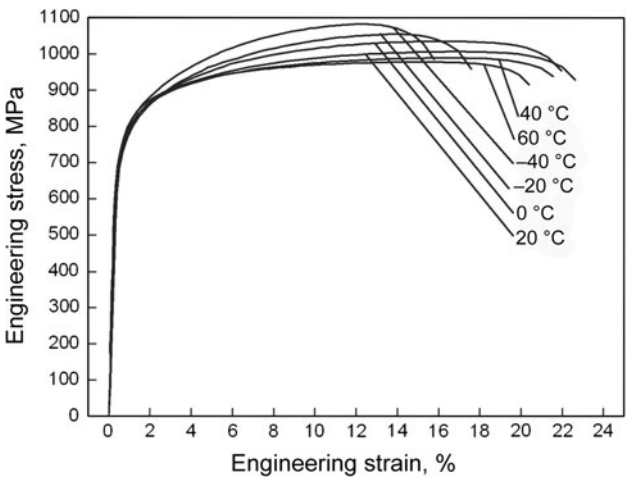

Fig. 11 Tensile engineering stress–strain curves at different temperatures

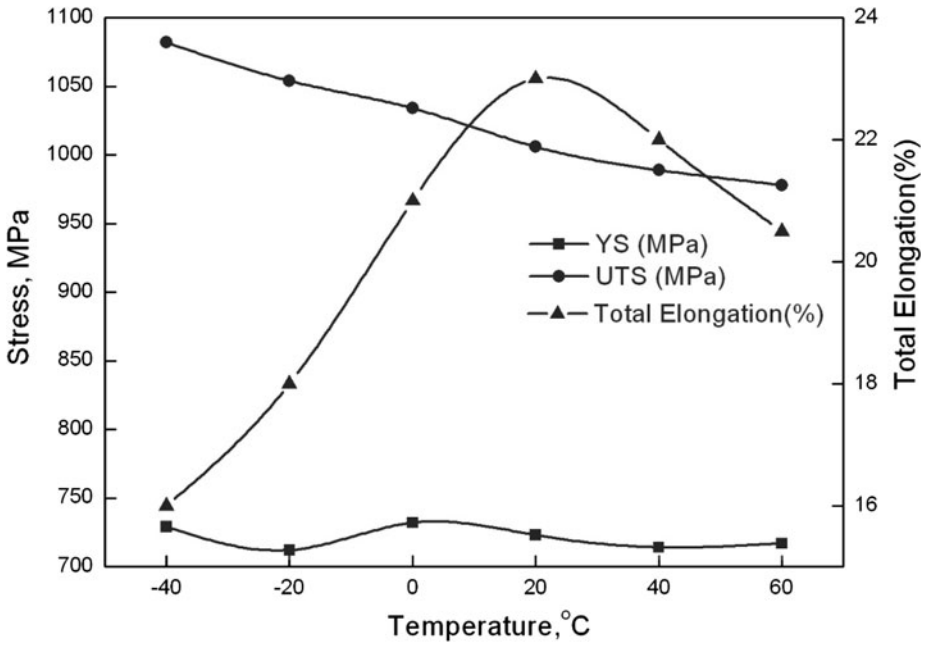

Fig. 12 Effect of test temperature on mechanical properties of Q&P 980 steel. *YS* yield strength; *UTS* ultimate tensile strength

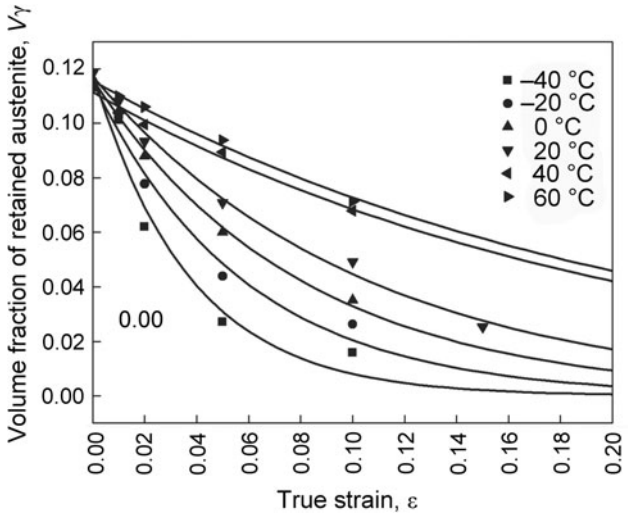

Fig. 13 Effect of strain and testing temperature on volume fraction of austenite

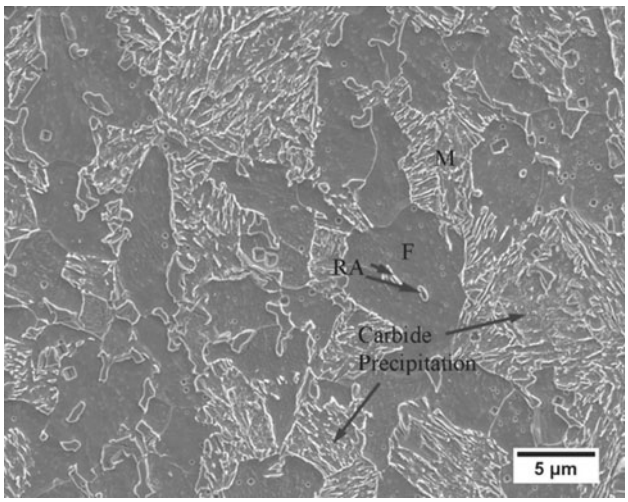

Fig. 14 Scanning electron micrograph of a Q&P steel containing intercritical ferrite (*F*), retained austenite (*RA*), and martensite (*M*), which is also associated with retained austenite and some carbides

x-ray diffraction (XRD), scanning electron microscopy, and electron backscatter diffraction (EBSD) [27]. Evolution of the volume fraction of retained austenite (V_γ) is shown in Fig. 13, determined from XRD of the studied Q&P sheet steel at different testing temperatures and strains. Generally, the transformation behavior of V_γ is roughly divided into two stages: a rapid decrease at low strains (stage I) and more sluggish decrease at high strains (stage II). However, in some cases, usually when tested at higher temperature, the first stage is less pronounced, and the retained austenite fraction decreases at an almost constant rate from the beginning of deformation. It should be noted here that the transformation rate ($dV_\gamma/d\varepsilon$) at lower testing temperature is faster than that at higher temperature, implying reduced mechanical stability of austenite at lower temperatures due to the smaller driving force needed for DIMT. This DIMT behavior at small strains is typical of stress-induced martensite transformation. For example, when tested at −40 °C (−40°F), almost all the retained austenite is transformed into martensite, and only approximately 3% remains after 5% strain. At 60 °C (140°F), however, most of the retained austenite remained untransformed even when deformed to a tensile strain of 10%. The transformation rates and the amount of retained austenite transformed at greater strains are less sensitive to testing temperature.

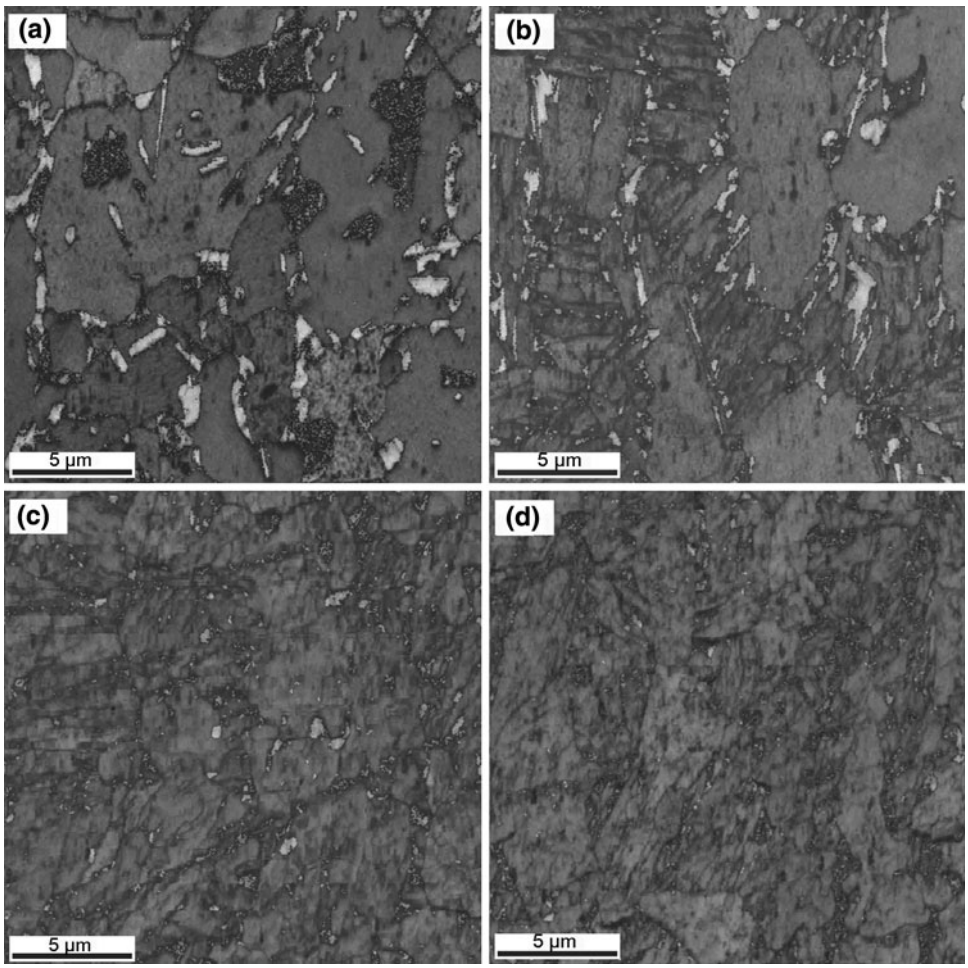

Fig. 15 EBSD maps of Q&P steel tension tested at 0 °C (32°F). *White* corresponds to face-centered cubic lattice (retained austenite). *Gray* scale indicates the image quality, where *darker-gray* scale indicates lower image quality (higher dislocation density). (**a**) 0, (**b**) 1, (**c**) 5, and (**d**) 10% strain

Table 3 Retained austenite volume fraction measured by XRD and EBSD

Method	Strain, %				
	Initial	1	2	5	10
XRD	0.116	0.105	0.088	0.060	0.035
EBSD[a]	0.112	0.104	0.080	0.053	0.03

[a] EBSD data with confidence index values greater than 0.05

Microstructure Evolution with Strain

Figure 14 shows a scanning electron micrograph of a Q&P steel after polishing and etching, showing apparently three characteristics: a rough surface structure corresponds to martensite, ferrite is relatively smooth with only slight surface structure, and the retained austenite areas appear smooth with a featureless surface structure, helping to distinguish it from ferrite and martensite. This steel was intercritically annealed before quenching, so a considerable ferrite fraction is present along with the Q&P constituent that consists of a mixture of martensite laths and retained austenite. Ideally, formable Q&P steels should not contain a substantial amount of iron carbide. The Q&P steel studied here was partitioned at 400 °C (752°F) for a few minutes, and, in this instance, the martensite regions also contained carbides. The presence of carbides is of importance because it implies that the cementite may not have fully dissolved, and the available carbon content does not fully contribute to the stabilization of the carbon-enriched austenite in the industrial processing conditions employed.

Microstructure evolution during tensile testing at different strain levels has been examined using EBSD. The microstructure of specimens undergoing different strains, that is, 0, 1, 5, and 10%, at 0 °C (32°F) was analyzed, and Fig. 15 shows the results of a combined image-quality map and gray-scale-coded phase map. Retained austenite is distributed both as thin films and as larger blocky regimes. It is clear that the retained austenite fraction decreases with increased strain, and the remaining austenite particles are mostly the finer ones. These results support the conclusion that finer retained austenite is more stable with deformation. According to Santofimia et al. [28], the darker-gray areas refer to regions that are likely martensite, based on poor image quality due to high dislocation density, while the lighter-gray areas perhaps represent ferrite. Another

Table 4 Resistance spot welding parameters

Thickness of base material		Welder	Weld electrode	Weld force		Cooling		Weld pulse
mm	in.			kN	lbf	L/min	gal/min	
1.6	0.06	Medium-frequency direct current	ISO 5821-16 × 20 (type B; diameter 6 mm, or 0.24 in.)	5.8	1305	2	0.5	3

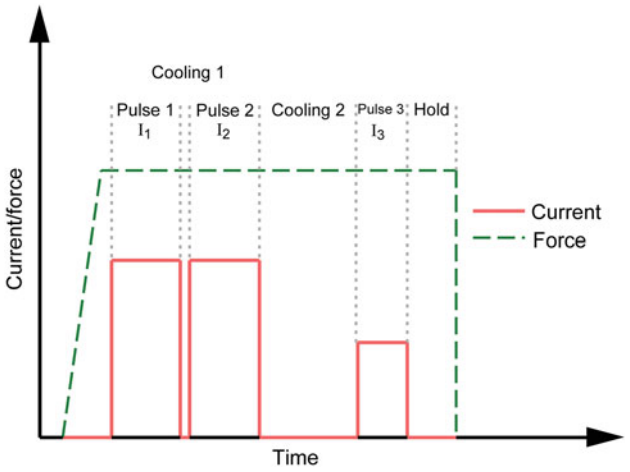

Fig. 16 Resistance spot welding pulsed current profile. Pulse 1 = pulse 2, $I_1 = I_2$; cooling 1 = 20 ms, cooling 2 = 200 ms; pulse 3 = 100 ms, $I_3 = 4.3$ kA; hold time = 100 ms

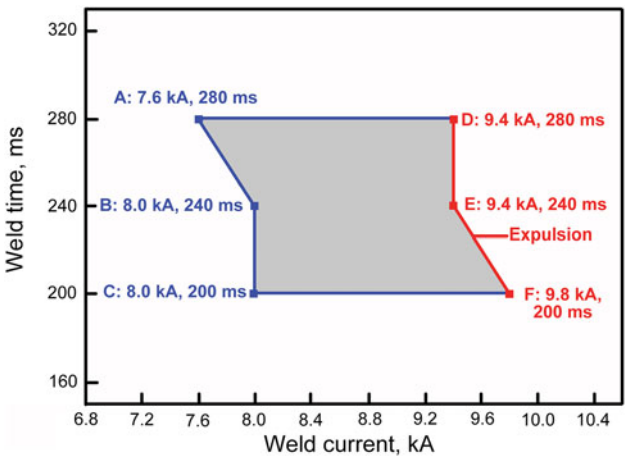

Fig. 17 Weld lobe for 1.6 mm (0.06 in.) Q&P 980

method [29] has also been shown to distinguish these phases by the character of the orientation relationships between them.

The volume fraction of retained austenite measured by EBSD, where all data with confidence index lower than 0.05 were excluded from the analysis as dubious, is a little lower than the one measured by XRD, as shown in Table 3. This behavior is consistent with other literature [30]. The discrepancies between results obtained using different methods may result from differences in sample preparation and penetration depths between the two techniques. During sample preparation, it is inevitable that some austenite transformed into martensite. The scale of the film austenite may also be below the resolution limits and cannot be identified.

Table 5 Spot weld strength for 1.6 mm (0.06 in.) Q&P 980

Point	Button size		Tensile shear strength		Cross-tension strength	
	mm	in.	kN	lbf	kN	lbf
A	6.5	0.256	26.7	6002	12.3	2765
B	6.2	0.244	26.0	5845	11.9	2675
C	6.0	0.236	23.9	5373	11.4	2563

Welding Properties

The Q&P 980 steel can be successfully welded with the correct set of parameters. Resistance spot welding, laser welding, and metal active gas (MAG) welding have produced good results.

Resistance Spot Welding

When resistance spot welded, Q&P 980 requires less current than conventional steels because it has higher electrical resistivity. On the other hand, due to its ultrahigh base material strength, Q&P 980 needs higher electrode forces than conventional steels that have equivalent thickness.

Weld Lobe

Resistance spot welding has been accomplished using the weld schedule shown in Table 4, with a pulsed current profile as shown in Fig. 16. Three types of weld times were

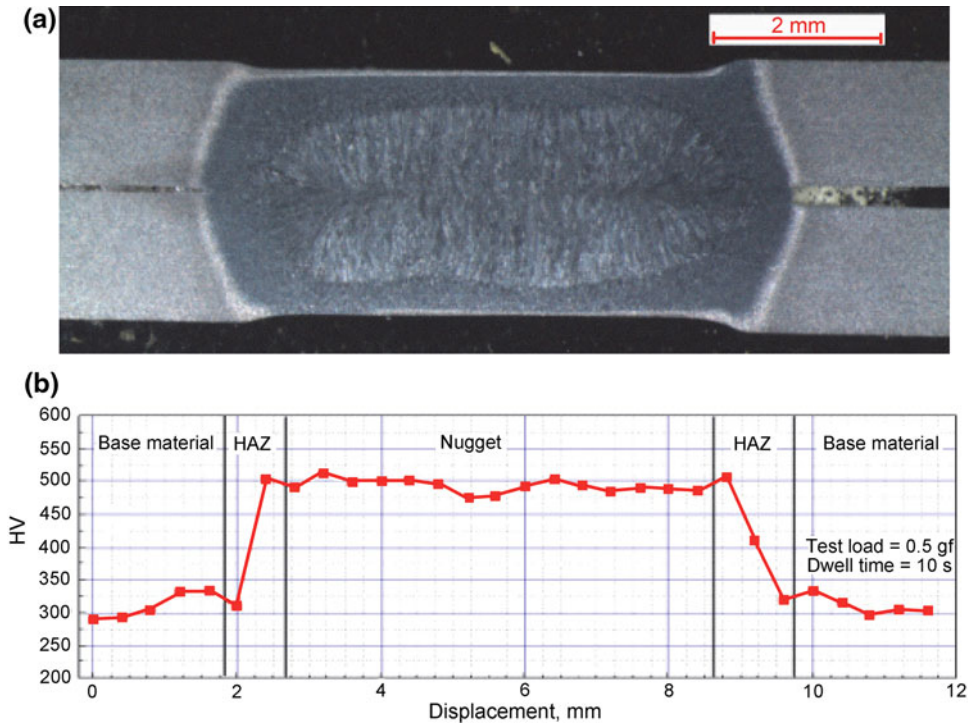

Fig. 18 Spot weld cross-sectional micrograph and microhardness profile for 1.6 mm (0.06 in.) Q&P 980. *HAZ* heat-affected zone

Table 6 Laser welding process parameters

Thickness		Power, kW	Weld speed		Defocus		Weld angle, °	Cover gas	Quantity of gas	
mm	in.		m/min	ft/min	mm	in.			L/min	gal/min
1.6	0.06	3	5	16	0	0	0	He	15	4.0

chosen to determine their welding current range. The actual weld times were pulse 1 = pulse 2 = 100 ms, pulse 1 = pulse 2 = 120 ms, and pulse 1 = pulse 2 = 140 ms. The weld lobe for 1.6 mm (0.06 in.) Q&P 980 is shown in Fig. 17. In this weld lobe, the minimum weld current is defined as the welding current needed to obtain a full button fracture mode when peel tested, and the maximum weld current is defined as the welding current when expulsion occurs. So, in the enclosed (shaded) zone of Fig. 17, the fracture modes of all spot welds were full button pullout when peel tested. The button size of these welds (in the shaded zone) ranged from 6.0 to 7.7 mm (0.24 to 0.30 in.).

As shown in Fig. 17, the weld current range is 8.0–9.8 kA (weld time: 200 ms), 8.0–9.4 kA (weld time: 240 ms), 7.6–9.4 kA (weld time: 280 ms). The weld lobe is wide enough for most applications.

Spot Weld Strength

The tensile shear strength and cross-tension strength of points "A," "B," and "C" (Fig. 17) are listed in Table 5. Points "A," "B," and "C" were located at the lower bound of the weld lobe, because it is known that, before expulsion happens, with weld current increasing, the spot weld strength increases with welding current. Overall, 1.6 mm (0.06 in.) Q&P 980 shows good spot weld strength performance.

Spot Weld Microstructure and Microhardness

A weld cross-sectional micrograph and microhardness profile for 1.6 mm (0.06 in.) Q&P 980 is shown in Fig. 18. No weld defects, such as cracks, shrinkage void, pore, no fusion, deep indentation, and so on, are noted. The weld nugget grew very well. The nugget microhardness is approximately 500 HV; its maximum hardness is 512 HV, while its minimum is 474 HV. The base material microhardness is approximately 300 HV. There is no obvious softened region in the heat-affected zone (HAZ).

Laser Welding

Laser welding has been successful using the welding parameters shown in Table 6.

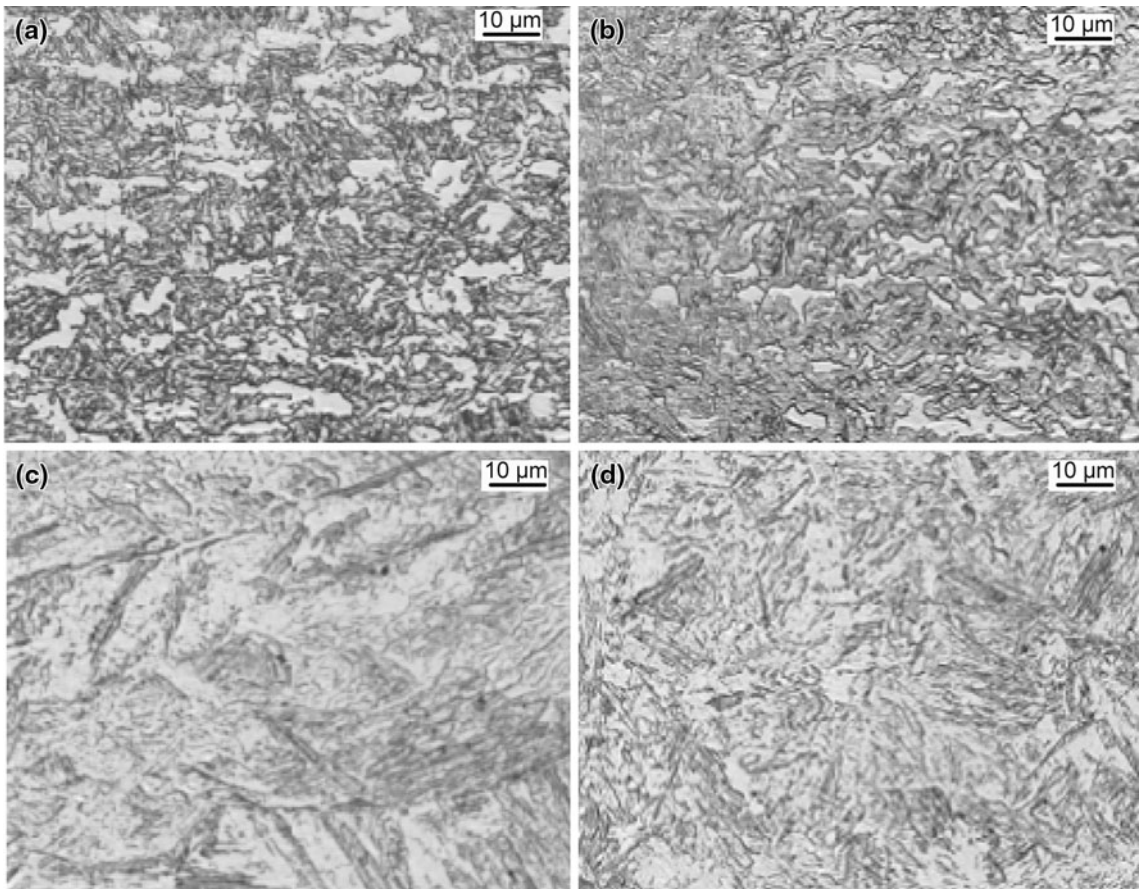

Fig. 19 Microstructures of 1.6 mm (0.06 in.) Q&P 980 laser-welded joint. (**a**) Base material. (**b**) Fine-grained HAZ. (**c**) Weld seam. (**d**) Coarse-grained HAZ

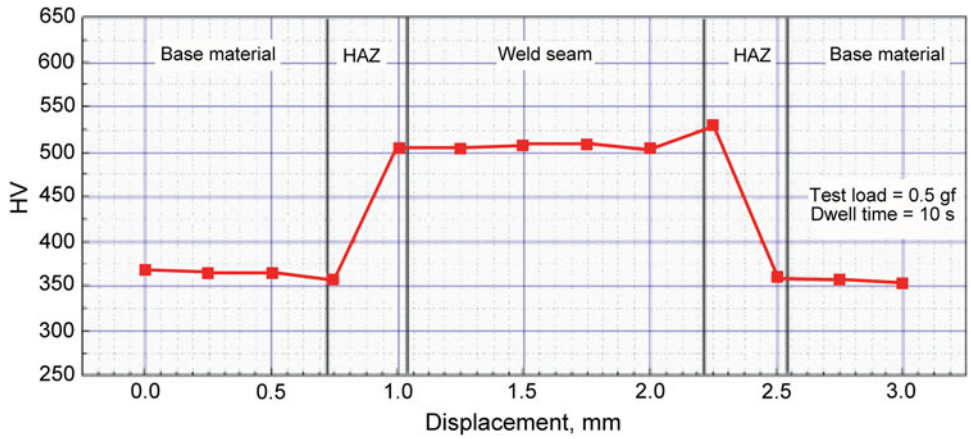

Fig. 20 Microhardness profile across 1.6 mm (0.06 in.) Q&P 980 laser-welded joint. *HAZ* heat-affected zone

Weld Joint Performance

The 1.6 mm (0.06 in.) Q&P 980 has good laser weldability. For the welding parameters in Table 6, the laser weld joint strength of 1.6 mm (0.06 in.) Q&P 980 was 1081 MPa (157 ksi), and the tensile failure was located in the base material far away from the weld seam and HAZ. Figure 19 shows the microstructure of a 1.6 mm Q&P 980 laser-welded joint. The weld seam zone is martensite, while the HAZ is martensite and ferrite. There were no weld defects found. Figure 20 is the microhardness profile of the 1.6 mm Q&P 980 laser-welded joint. Microhardnesses in both the welded seam and HAZ are higher than in the base material, and there is no obvious softened region in the HAZ.

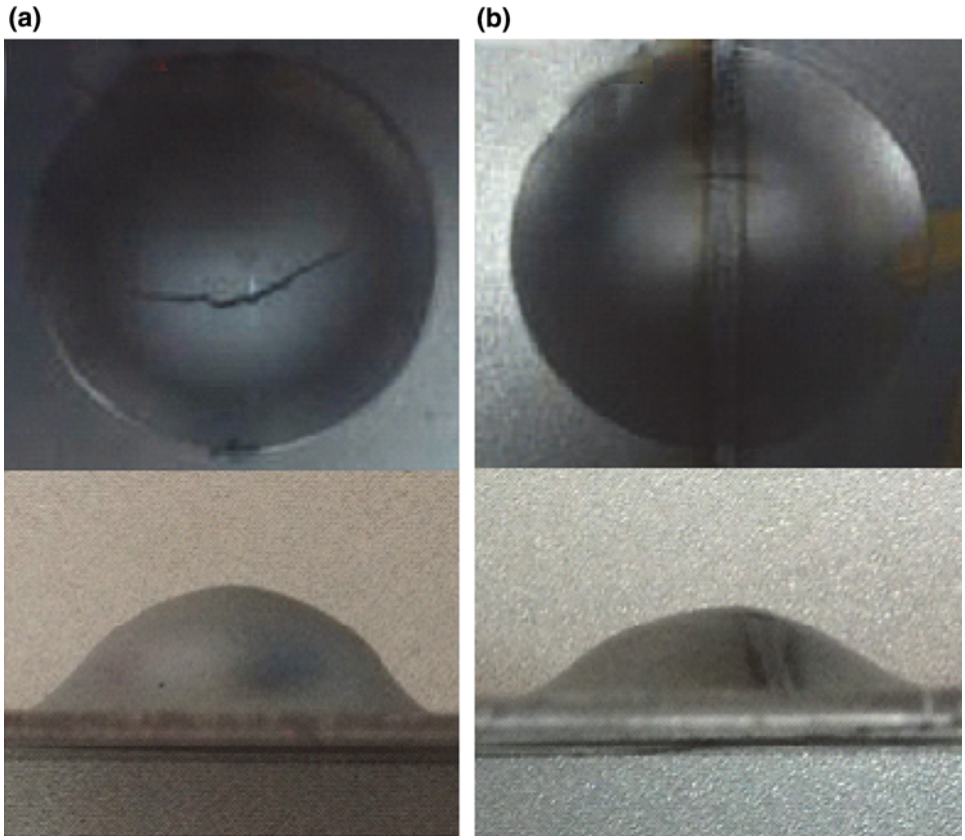

Fig. 21 Photographs of Erichsen test specimens for (**a**) base material and (**b**) laser-welded seam

Table 7 MAG welding process parameters

Thickness of base material		Welding speed		Energy input		Cover gas	Filler material	Quantity of gas		Blowpipe distance	
mm	in.	cm/min	in./min	kJ/cm	Btu/in.			L/min	gal/min	mm	in.
1.6	0.06	35	14	3.6	8.7	80% Ar + 20% CO_2	ER110S	14	3.7	12	0.5

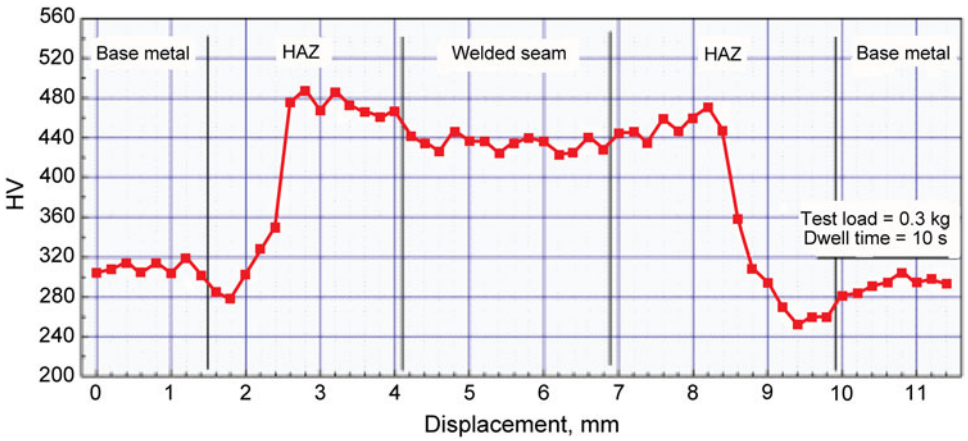

Fig. 22 Microhardness profile across 1.6 mm (0.06 in.) Q&P 980 metal-active-gas-welded joint. *HAZ* heat-affected zone

The laser weld seam for Q&P 980 has good stretchability. Figure 21 shows Erichsen cups after testing the base material and weld seam of 1.6 mm (0.06 in.) Q&P 980. The Erichsen test performance describes the stretchability. Using this test, the Erichsen value for the laser weld seam was 7.34 mm (0.29 in.), approximately 70% of the value for the base

material (10.3 mm, or 0.4 in.), and the fracture direction in the Erichsen test was perpendicular to the laser-welded seam.

MAG Welding

MAG welding was successful using the welding parameters shown in Table 7.

Weld Joint Performance

Despite the greater alloy content used for Q&P 980, there were no more welding defects than observed with mild steel MAG welds. For the parameters listed in Table 7, the MAG weld strength of 1.6 mm (0.06 in.) Q&P 980 is 991 MPa (144 ksi). Figure 22 shows the microhardness profile of the 1.6 mm Q&P 980 MAG weld joint. The microhardness of both the welded seam and HAZ is less than 500 HV, and there is no obvious softened region in HAZ.

Acknowledgments The authors would like to thank Yong Zhong, Weijun Feng, and Xinyan Jin for providing previously unpublished data and for their assistance in the preparation of this article.

References

1. J.G. Speer, D.K. Matlock, B.C. De Cooman, J.G. Schroth, Carbon partitioning into austenite after martensite transformation. Acta Mater. **51**, 2611–2622 (2003)
2. J.G. Speer, D.V. Edmonds, F.C. Rizzo, D.K. Matlock, Partitioning of carbon from supersaturated plates of ferrite, with application to steel processing and fundamentals of the bainite transformation. Curr. Opin. Solid State Mater. Sci. **8**, 219–237 (2004)
3. J.G. Speer, D.K. Matlock, B.C. DeCooman, J.G. Schroth, Comments on "on the definitions of paraequilibrium and orthoequilibrium" by M. Hillert and J. Agren, *Scr. Mater.,* Vol 50, 2004, p 697–699. Scr. Mater. **52**, 83–85 (2004)
4. D.K. Matlock, J.G. Speer, Design considerations for the next generation of advanced high strength sheet steels, in *Proceedings of the Third International Conference on Structural Steels*, ed. by H.C. Lee (The Korean Institute of Metals and Materials, Seoul, 2006), pp. 774–781
5. J.G. Speer, F.C. Rizzo Assunção, D.K. Matlock, D.V. Edmonds, The quenching and partitioning process: background and recent progress. Mater. Res. **8**, 417–423 (2005)
6. D.V. Edmonds, K. He, M.K. Miller, F.C. Rizzo, A. Clarke, D.K. Matlock, et al., Microstructural features of quenching and partitioning: a new martensitic steel heat treatment, in *Fifth International Conference on Processing and Manufacturing of Advanced Materials*, Vancouver, 2006, ed. by T. Chandra, K. Tsuzaki, M. Militzer, C. Ravindran, pp. 4819–4825
7. D.V. Edmonds, K. He, F.C. Rizzo, B.C. De Cooman, D.K. Matlock, J.G. Speer, Quenching and partitioning martensite—a novel steel heat treatment. Mater. Sci. Eng. A **438–440**, 25–34 (2006)
8. K. He, D.V. Edmonds, J.G. Speer, D.K. Matlock, F.C. Rizzo, Microstructural characterisation of steel heat-treated by the novel quenching and partitioning process, in *EMC 2008 14th European Microscopy Congress,* Aachen, Sept 1–5, 2008 (Springer, Berlin, 2008), pp. 429–430
9. S.S. Nayak, R. Anumolu, R.D.K. Misra, K.H. Kim, D.L. Lee, Microstructure-hardness relationship in quenched and partitioned medium-carbon and high-carbon steels containing silicon. Mater. Sci. Eng. A **498**, 442–456 (2008)
10. M.J. Santofimia, L. Zhao, R. Petrov, J. Sietsma, Characterization of the microstructure obtained by the quenching and partitioning process in a low-carbon steel. Mater. Charact. **59**, 1758–1764 (2008)
11. C.Y. Wang, J. Shi, W.Q. Cao, H. Dong, Characterization of microstructure obtained by quenching and partitioning process in low alloy martensitic steel. Mater. Sci. Eng. A **527**, 3442–3449 (2010)
12. J.G. Speer, E. De Moor, K.O. Findley, D.K. Matlock, B.C. De Cooman, D.V. Edmonds, Analysis of microstructure evolution in quenching and partitioning automotive sheet steel. Metall. Mater. Trans. A **42**, 3591–3601 (2011)
13. G. Thomas, J. Speer, D. Matlock, J. Michael, Application of electron backscatter diffraction techniques to quenched and partitioned steels. Microsc. Microanal. **17**, 368–373 (2011)
14. E. De Moor, S. Lacroix, A.J. Clarke, J. Penning, J.G. Speer, Effect of retained austenite stabilized via quench and partitioning on the strain hardening of martensitic steels. Metall. Mater. Trans. A **39**, 2586–2589 (2008)
15. M.J. Santofimia, L. Zhao, J. Sietsma, Model for the interaction between interface migration and carbon diffusion during annealing of martensite–austenite microstructures in steels. Scr. Mater. **59**, 159–162 (2008)
16. M.J. Santofimia, J.G. Speer, A.J. Clarke, L. Zhao, J. Sietsma, Influence of interface mobility on the evolution of austenite–martensite grain assemblies during annealing. Acta Mater. **57**, 4548–4557 (2009)
17. Y. Takahama, M.J. Santofimia, M.G. Mecozzi, L. Zhao, J. Sietsma, Phase field simulation of the carbon redistribution during the quenching and partitioning process in a low-carbon steel. Acta Mater. **60**, 2916–2926 (2012)
18. D.K. Matlock, J.G. Speer, Processing opportunities for new advanced high-strength sheet steels. Mater. Manuf. Process. **25**, 7–13 (2010)
19. G.A. Thomas, J.G. Speer, D.K. Matlock, Considerations in the application of the quenching and partitioning concept to hot rolled AHSS production. Iron Steel Technol. **5**, 209–217 (2008)
20. G.A. Thomas, J.G. Speer, D.K. Matlock, Quenched and partitioned microstructures produced via Gleeble simulations of hot-strip mill cooling practices. Metall. Mater. Trans. A **42**, 3652–3659 (2011)
21. L. Wang, W. Li, W. Feng, Industry trials of C–Si–Mn steel treated by Q&P concept in Baosteel. Presented at SAE International Congress, Detroit, 2010
22. L. Wang, X. Jin, H. Qian, Recent development of galvanizing sheet steels in Baosteel, in *Proceedings of Galvatech 2011: Eighth International Conference on Zinc and Zinc Alloy Coated Sheet Steel*, Genova, 2011
23. L. Wang, W. Feng, Development and application of Q&P sheet steels, in *Advanced Steels: The Recent Scenario in Steel Science and Technology*, ed. by W. Yuqing, D. Han, G. Yong (Springer, New York, 2011), p. 255
24. A.W. Hudgins, Shear fracture in bending of advanced high strength steels, Ph.D. thesis, MT-SRC-010-008, Colorado School of Mines, Golden, 2010
25. D.K. Matlock, J.G. Speer, in *Third Generation of AHSS: Microstructure Design Concepts*, ed. by A. Haldar, S. Suwas, D. Bhattacharjee (Springer, London, 2009), p. 185
26. J.G. Speer, A.M. Streicher, D.K. Matlock, F. Rizzo, G. Krauss, *Austenite Formation and Decomposition*, ed by E.B. Damm, M.J. Merwin (TMS, Warrendale, 2003), p. 505
27. A.J. Clarke, Ph.D. thesis, Colorado School of Mines, Golden, 2006

28. M.J. Santofimia, L. Zhao, J. Sietsma, Microstructural evolution of a low-carbon steel during application of quenching and partitioning heat treatments after partial austenitization. Metall. Mater. Trans. A **40**, 46–57 (2009)
29. S. Zaefferer, J. Ohlert, W. Bleck, A study of microstructure, transformation mechanisms and correlation between microstructure and mechanical properties of a low alloyed TRIP steel. Acta Mater. **52**, 2765–2778 (2004)
30. T. Bhattacharyya, S.B. Singh, S. Das, A. Haldar, D. Bhattacharjee, Development and characterisation of C–Mn–Al–Si–Nb TRIP aided steel. Mater. Sci. Eng. A **528**, 2394–2400 (2011)